TRANSLATIONAL AND ROTATIONAL DIFFUSION CONSTANTS OF TOBACCO MOSAIC VIRUS FROM RAYLEIGH LINEWIDTHS

HERMAN Z. CUMMINS, FRANCIS D. CARLSON, THOMAS J. HERBERT, *and* GARY WOODS

From the Thomas C. Jenkins Department of Biophysics, Johns Hopkins University, Baltimore, Maryland 21218

ABSTRACT The translational and rotational diffusion constants of tobacco mosaic virus (TMV) have been determined from homodyne and heterodyne measurements of the spectrum of laser light scattered from dilute aqueous solutions of TMV. Our results for the translational and rotational constants respectively, reduced to 20°C, are: $D_T = 0.280 \pm 0.006 \times 10^{-7}$ cm²/sec, and $D_R = 320 \pm 18$ sec^{-1}. We include a theoretical derivation of the spectrum of light scattered from rod-shaped molecules which reproduces results obtained previously by Pecora, but which is specialized at the outset to the problem of dilute solutions so that simple single-particle correlation functions may be utilized. An analysis of the photocurrent spectrum for both the homodyne and heterodyne detection schemes is given. Various data reduction schemes utilized in the analysis of our spectra are described in some detail, and our results are compared with values of the diffusion constants obtained from other experiments.

INTRODUCTION

For many years the measurement of light scattered by dilute solutions of polymers or macromolecules has provided an important technique for molecular weight determination (1–3).

Until recently, only the intensity and angular dependence of the scattering were considered. However, it was recognized several years ago that the spectrum of the scattered light contains additional information related to the hydrodynamic properties of the scatterers—i.e., the translational and rotational diffusion constants. A time-dependent correlation function formalism first developed by Van Hove (4) for neutron scattering was extended to light scattering by Komarov and Fisher (5) and by Pecora (6). Pecora's basic paper has subsequently been extended to cover additional macromolecular problems (7, 8).

In 1964, the spectrum of laser light scattered by dilute solutions of polystyrene

latex spheres was observed, and was indeed found to exhibit broadening due to particle diffusion, in good quantitative agreement with the theory (9). Other measurements of the polystyrene latex spectrum have subsequently been reported by other groups who obtained essentially equivalent results (10, 11).

In 1967, Rayleigh linewidth measurements were reported for a series of biological macromolecules by Dubin, Lunacek, and Benedek (10). These investigators analyzed their data in terms of a single Lorentzian fit, and found serious discrepancies for tobacco mosaic virus (TMV), the most highly anisotropic molecule that they studied.

Pecora had shown that the spectrum of light scattered from anisotropic molecules would be more complex than the scattering from spheres (where the spectrum consists of a single Lorentzian) and had in fact deduced general expressions for rod-shaped molecules such as TMV (6, 8). Although no one has heretofore attempted the more complex analysis implied by Pecora's expressions, the incentive for doing so lies in the fact that the analysis can simultaneously produce values for both the translational *and* rotational diffusion constants.

In this paper we report a new experimental study of light scattering by TMV. In this study we have utilized Pecora's full theoretical treatment and have extracted values for the translational and rotational diffusion coefficients which agree well with the results of previous experiments.

In part I, we give a derivation of the light scattering spectrum, $I(\omega)$. Although the results are equivalent to those of Pecora, we wish to show that considerable simplification of the theory is achieved by utilizing the statistical independence of the scatterers at the outset. For those primarily interested in dilute macromolecular solutions this approach is much easier than the more general approach utilized by Pecora. Numerical tables have been prepared for use in the study of other macromolecular systems[1] and are available on request.

In part II, we discuss the spectroscopic techniques, and part III describes the instrumentation. Part IV takes up the TMV experiment discussing sample preparation, data collection, and analysis, and part V covers the results and comparison with other published data.

I. THE SPECTRUM OF LIGHT SCATTERED BY A DILUTE SOLUTION OF MACROMOLECULES

Consider a large volume (filled with a solvent) which contains N identical scatterers.

The volume is illuminated with a monochromatic plane wave of frequency ω_0 polarized perpendicular to the scattering plane, and light scattered at an angle ψ is observed at a distant point R_0 (see Fig. 1).

---

[1] Very recently Pecora has independently performed some of the same numerical evaluation procedures performed here (8).

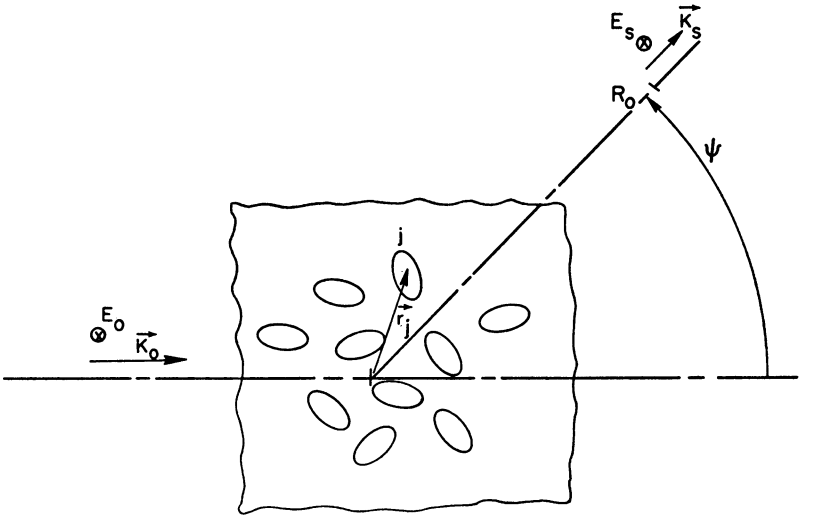

FIGURE 1 Geometry of the scattering system for which power spectra are to be derived.

The field observed at R_0 due to the j^{th} scatterer will be

$$E_j = A_j e^{i\phi_j} e^{-i\omega_0 t} \tag{1}$$

where the amplitude A_j may depend on orientation. If we let the position of the j^{th} scatterer be $\mathbf{r}_j$, and we choose the phase $\phi = 0$ for a scatterer at the origin, then:

$$\phi_j = (\mathbf{K}_0 - \mathbf{K}_s)\cdot\mathbf{r}_j = \mathbf{q}\cdot\mathbf{r}_j \tag{2}$$

where $\mathbf{K}_0$ and $\mathbf{K}_s$ are the wave vectors of the incident and scattered light respectively If the scatterer moves slowly ($v \ll c$), then $|\mathbf{K}_0| \approx |\mathbf{K}_s|$ so that

$$|\mathbf{q}| \approx 2|\mathbf{K}_0| \sin(\psi/2) = (4\pi n_0/\lambda_0)\sin(\psi/2) \tag{3}$$

where n_0 is the refractive index of the solvent. For the total scattered field at R_0 we have

$$E_s = \sum_{j=1}^{N} E_j = \sum_{j=1}^{N} A_j(t) e^{i\mathbf{q}\cdot\mathbf{r}_j} e^{-i\omega_0 t} \tag{4}$$

The total average scattered intensity is given by:

$$I_s = \langle |E_s|^2 \rangle$$

where the angular brackets denote a time average. Since the scatterers are not correlated, all cross terms average to zero, whence

$$I_s = \langle \sum_j |A_j|^2 \rangle = N\langle |A|^2 \rangle \tag{5}$$

In order to compute the spectrum of the scattered light, we utilize the Wiener-Khintchine theorem:

$$I(\omega) = \frac{1}{2\pi} \int_{-\infty}^{\infty} C(\tau) e^{i\omega\tau} \, d\tau \tag{6}$$

where we define $C(-\tau) = C^*(\tau)$.
The autocorrelation function $C(\tau)$ is defined by

$$C(\tau) = \langle E_s^*(t) E_s(t + \tau) \rangle \tag{7}$$

Combining Equations 4 and 7,

$$C(\tau) = \langle \sum_{j=1}^{N} A_j^*(t) e^{-i\mathbf{q}\cdot\mathbf{r}_j(t)} e^{i\omega_0 t} \sum_{l=1}^{N} A_l(t + \tau) e^{i\mathbf{q}\cdot\mathbf{r}_l(t+\tau)} e^{-i\omega_0(t+\tau)} \rangle \tag{8}$$

We now invoke the statistical independence of the scatterers to eliminate cross terms ($j \neq l$), the statistical independence of position and orientation to factor amplitudes and phases, and finally the fact that the N scatterers are identical so that each must have the same autocorrelation function. Thus,

$$C(\tau) = N e^{-i\omega_0\tau} \langle A^*(t) A(t + \tau) \rangle \langle e^{-i\mathbf{q}\cdot\mathbf{r}(t)} e^{i\mathbf{q}\cdot\mathbf{r}(t+\tau)} \rangle \tag{9}$$

Since we are now dealing with single particle correlation functions, the subscripts have been eliminated. Equation 6 then becomes:

$$I(\omega) = N \frac{1}{2\pi} \int_{-\infty}^{+\infty} e^{i(\omega-\omega_0)\tau} \, [C_A(\tau)][C_\phi(\tau)] \, d\tau \tag{10}$$

where

$$[C_A(\tau)] = \langle A^*(t) A(t + \tau) \rangle$$

$$[C_\phi(\tau)] = \langle e^{-i\mathbf{q}\cdot\mathbf{r}(t)} e^{i\mathbf{q}\cdot\mathbf{r}(t+\tau)} \rangle$$

The separation of orientation and position is not rigorously correct, and should be considered as a simplifying approximation.

SPHERICAL SCATTERERS

If the scatterers are spherical, then the scattering amplitude $A(t)$ is a constant and the amplitude autocorrelation function $[C_A(\tau)] = |A|^2$. From Equation 10, the spectrum is thus given by

$$I(\omega) = N |A|^2 \frac{1}{2\pi} \int_{-\infty}^{+\infty} e^{i(\omega-\omega_0)\tau} \, [C_\phi(\tau)] \, d\tau \tag{11}$$

The phase autocorrelation function $[C_\phi(\tau)]$ is analyzed for three cases in the Appendix where we find:

A: Static scatterers (fixed random positions)

$$[C_\phi(\tau)] = 1 \tag{12 a}$$

B: Scatterers moving with constant velocity $\mathbf{v}$

$$[C_\phi(\tau)] = e^{i\mathbf{q}\cdot\mathbf{v}\tau} \tag{12 b}$$

C: Scatterers undergoing translational diffusion characterized by the diffusion constant D_T

$$[C_\phi(\tau)] = e^{-D_T q^2 \tau} \tag{12 c}$$

For each case, the phase autocorrelation function can then be put into Equation 11 to find the spectrum.

A: Static scatterers

$$I(\omega) = N \mid A \mid^2 \delta(\omega - \omega_0) \tag{13 a}$$

so the total scattered intensity $N \mid A \mid^2$ appears at the frequency of the incident light ω_0, and the scattering is perfectly elastic.

B: Constant velocity $\mathbf{v}$

$$I(\omega) = N \mid A \mid^2 \delta(\omega - \omega_0 + \mathbf{q}\cdot\mathbf{v}) \tag{13 b}$$

Again the total scattered intensity appears at a single frequency, but now is Doppler shifted to $\omega = \omega_0 - \mathbf{q}\cdot\mathbf{v}$

C: Translational diffusion

$$I(\omega) = N \mid A \mid^2 \cdot \frac{1}{2\pi} \int_{-\infty}^{+\infty} e^{i(\omega-\omega_0)\tau} e^{-D_T q^2 \tau}\, d\tau$$

$$I(\omega) = N \mid A \mid^2 \left\{ \frac{D_T q^2/\pi}{(\omega - \omega_0)^2 + (D_T q^2)^2} \right\} \tag{13 b}$$

The quantity in brackets in Equation 13 c is a normalized Lorentzian centered at $\omega = \omega_0$, with half-width at half-maximum of:

$$\Delta\omega_{\frac{1}{2}} = D_T q^2 \tag{14}$$

Equation 13 c for the quasielastic scattering from scatterers undergoing translational diffusion has been utilized in the analysis of the experiments reported in references 9–11. For the case of spheres in water at 20°C, assuming $D_T = kT/6\pi\eta r$

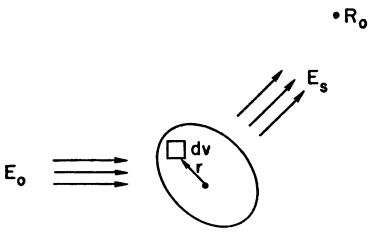

FIGURE 2 Geometry of a single scatterer for which the scattered amplitude is determined in the Rayleigh-Gans approximation.

(Stokes's law) and $\lambda_0 = 6328$A it was shown in reference 9 that the linewidth (Equation 14) becomes

$$\Delta\omega_{\frac{1}{2}} = \frac{49\ \pi \sin^2 (\psi/2)}{r} \tag{15}$$

where r is the radius of the sphere in microns.

The Scattering Amplitude A

Many biologically important macromolecules are physically anisotropic but optically isotropic. For optically isotropic particles which are very small compared to the wavelength, the scattering amplitude is *independent* of orientation, and the spectrum will be identical to that of spheres regardless of the shape (Rayleigh limit).

If the scatterer is too large to meet the Rayleigh criterion ($L \ll \lambda$), but its refractive index (n) is not too different from that of the solvent (n_0), then it may meet the weaker Rayleigh-Gans criterion (2, 3, 12):

$$2K_0L(n - n_0) \ll 1 \tag{16}$$

The Rayleigh-Gans procedure is simply to imagine that each element of the scatterer is subjected to the incident field $E_0 e^{i(\mathbf{K}_0 \cdot \mathbf{r} - \omega_0 t)}$, which produces a local dipole moment, and then sum up the scattered field by integrating over the scatterer (see Fig. 2). The amplitude of the scattered field at the distant point R_0 is then:

$$A = \int_v A_0\, e^{i\mathbf{q}\cdot\mathbf{r}}\, dV = A_0 V \left\{ \frac{1}{V} \int_v e^{i\mathbf{q}\cdot\mathbf{r}}\, dV \right\}$$

where A_0 is the scattered amplitude per unit volume of scatterer in the Rayleigh limit $L \ll \lambda$. $|A_0|^2$ is evaluated in reference 3

$$|A_0|^2 = \frac{I_0 K_0^4}{(2\pi R_0)^2} \left(\frac{n}{n_0} - 1 \right)^2 = \frac{4\pi^2 I_0}{R_0^2 \lambda_{0\text{vac}}^4}\, n_0\, (n - n_0)^2 \tag{17}$$

The factor $\{(1/V)\int_v e^{i\mathbf{q}\cdot\mathbf{r}}\, dV\} = f_q$ is a normalized "form factor." In the limit $q \to 0 (\psi \to 0)$, $f_q = 1$. In general $f_q \leqq 1$. For spherical scatterers,

$$f_q(\text{sphere}) = \sin(qb)/(qb) \tag{18}$$

where b is the radius.

Rigid Rods

For rigid rod-shaped scatterers, the form factor f_q can be readily evaluated (3, 12).

Let θ be the angle between the rod axis and $\mathbf{q}$. If a, the cross-sectional area of the rod is $\ll \lambda^2$

$$f_q = \frac{1}{V}\int e^{i\mathbf{q}\cdot\mathbf{r}}\,dV = \frac{a}{V}\int_{-L/2}^{L/2} e^{iql\cos\theta}\,dl \tag{19}$$

$$f_q = \sin\left(\frac{qL}{2}\cos\theta\right)\Big/\left(\frac{qL}{2}\cos\theta\right)$$

where L is the length of the rod.

If the rod changes its orientation randomly in time, f will be given by

$$f = f_0 + f_1(t)$$

where $f_0 = \langle f\rangle$ is the time average part of f, and $\langle f_1(t)\rangle = 0$.

The amplitude autocorrelation function (from Equation 10)

$$[C_A(\tau)] = \langle A^*(t)A(t+\tau)\rangle$$

will thus be given by:

$$\begin{aligned}[C_A(\tau)] &= |A_0V|^2\langle[f_0 + f_1(t)][f_0 + f_1(t+\tau)]\rangle \\ &= |A_0V|^2\{f_0^2 + \langle f_1(t)f_1(t+\tau)\rangle\}\end{aligned} \tag{20}$$

Combining Equations 10 and 20,

$$\begin{aligned}I(\omega) = {} & N|A_0V|^2\cdot\frac{1}{2\pi}\int_{-\infty}^{\infty} f_0^2 e^{i(\omega-\omega_0)\tau}[C_\phi(\tau)]\,d\tau \\ & + N|A_0V|^2\cdot\frac{1}{2\pi}\int_{-\infty}^{+\infty} e^{i(\omega-\omega_0)\tau}\langle f_1(t)f_1(t+\tau)\rangle[C_\phi(\tau)]\,d\tau\end{aligned}$$

Thus the spectrum consists of two parts: The first (spherical) depends only on $[C_\phi(\tau)]$ and is equivalent to the spectrum of spherical scatterers considered earlier. The second (modified) depends on both $[C_\phi(\tau)]$ and $\langle f_1(t)f_1(t+\tau)\rangle$ and is determined by both the translational *and* orientational dynamics of the scatterer.

Assuming only random orientations, the power in the "spherical" and "modified" parts of the spectrum can be evaluated without specifying the dynamics explicitly.

Since $f = f_0 + f_1(t), f_0 = \langle f \rangle$ and $\langle f_1(t) \rangle = 0$,

$$\langle f_1^2 \rangle = \langle f^2 \rangle - \langle f \rangle^2 \tag{22}$$

$$\langle f \rangle = \frac{1}{4\pi} \int_\Omega f(\theta)\, d\Omega = \frac{1}{4\pi} \int_\theta \int_\phi \left[\sin\left(\frac{qL}{2} \cos\theta\right) \Big/ \left(\frac{qL}{2} \cos\theta\right) \right] \sin\theta\, d\theta\, d\phi$$

$$\langle f \rangle = \frac{2}{qL} \int_0^{qL/2} \frac{\sin x}{x}\, dx \tag{23}$$

Similarly

$$\langle f^2 \rangle = \frac{2}{qL} \int_0^{qL/2} \frac{\sin^2 x}{x^2}\, dx = \frac{2}{qL} \int_0^{qL/2} \frac{\sin x}{x}\, dx - \frac{\sin\,(qL/2)}{(qL/2)} \tag{24}$$

Letting $h = qL/2$ and

$$\mathrm{Si}\,(\beta) = \int_0^\beta \frac{\sin x}{x}\, dx$$

$$\frac{I\ (\text{spherical})}{N(A_0V)^2} = \langle f \rangle^2 = [\mathrm{Si}\,(h)/h]^2$$

$$\frac{I\ (\text{modified})}{N(A_0V)^2} = \mathrm{Si}\,(2h)/h - [\sin\,(h)/h]^2 - [\mathrm{Si}\,(h)/h]^2$$

$$\frac{I(\text{total})}{N(A_0V)^2} = \langle f^2 \rangle = \mathrm{Si}\,(2h)/h - [\sin\,(h)/h]^2 \tag{25}$$

To complete our derivation of the spectrum $I(\omega)$, the dynamics of the orientational motion must be specified so that $C_A(\tau)$, the amplitude autocorrelation function, can be determined. We assume that the rod-shaped scatterer undergoes rotational diffusion due to collisions with the solvent molecules. Accordingly the time evolution of the ensemble averaged probability of the orientation of the scatterer is described by the solutions of the classical rotational diffusion equation under the appropriate initial conditions. As in the case of translational diffusion these conditions are specified in terms of a conditional probability, $G(\Omega_\tau, \Omega_0)$, that a scatterer oriented into Ω_0 at time 0 will be oriented into Ω_τ at time τ. With this choice of initial conditions and by the same arguments of homogeneity, isotropy and stationarity used previously it follows that:

$$C_A(\tau) = \frac{1}{4\pi} \int_{\Omega 0} \int_{\Omega_\tau} A(\Omega_0) A(\Omega_\tau) G(\Omega_0, \Omega_\tau)\, d\Omega_\tau\, d\Omega_0 \tag{26 a}$$

where for a thin rod in the Rayleigh-Gans approximation

$$A(\Omega) = A_0 \int e^{i\mathbf{q}\cdot\mathbf{r}}\, dv$$

and

$$G(\Omega_\tau, \Omega_0) = \sum_{lm} Y_l^{m*}(\Omega_0) Y_l^m(\Omega_\tau) e^{-l(l+1) D_R \tau}$$

The spherical harmonics, Y_l^m, arise in the solution because the rotational diffusion equation is formally equivalent to the Legendre equation. Substitution of $A(\Omega)$ and $G(\Omega_\tau, \Omega_0)$ in Equation (26 *a*) and integration gives:

$$C_A(\tau) = (A_0 V)^2 \sum_{\substack{l=0 \\ \text{even}}}^{\infty} B_l e^{-l(l+1) D_R \tau} \qquad (26\,b)$$

where

$$B_l = (2l + 1) \left[\frac{1}{h} \int_0^h \frac{J_l(x)}{(x)} dx\right]^2$$

$$h = qL/2 \text{ and } J_l(x) = \sqrt{\frac{\pi x}{2}} J_{l+\frac{1}{2}}(x)$$

as was first shown by Pecora (6). We can now compute the total spectrum for rod-shaped scatterers undergoing simultaneous rotational and translational diffusion. From Equation 10,

$$I(\omega) = N \cdot \frac{1}{2\pi} \int_{-\infty}^{+\infty} e^{i(\omega - \omega_0)\tau} [C_A(\tau)][C_\phi(\tau)]\, d_\tau$$

and Equations 12 *c* and 26 for $[C(_\phi\tau)]$ and $[C_A(\tau)]$, we find:

$$I(\omega) = N(A_0 V)^2 \cdot \frac{1}{2\pi} \int_{-\infty}^{+\infty} e^{i(\omega - \omega_0)\tau} \{e^{-D_T q^2 \tau} \sum_{\substack{l=0 \\ \text{even}}}^{\infty} B_l e^{-l(l+1) D_R \tau}\}\, d_\tau$$

$$I(\omega) = N(A_0 V)^2 \sum_{\substack{l=0 \\ \text{even}}}^{\infty} B_l \left\{\frac{1}{2\pi} \int_{-\infty}^{+\infty} \exp\,[i(\omega - \omega_0)\tau] \right.$$

$$\left. \exp\,[-(D_T q^2 + l(l+1) D_R)\tau]\, d\tau \right\} \qquad (27)$$

The quantity in braces { } is a normalized Lorentzian centered at $\omega = \omega_0$, of half-width at half maximum:

$$\Delta\omega_{\frac{1}{2}} = D_T q^2 + l(l+1) D_R$$

Letting $L(\beta)$ represent a normalized Lorentzian of half-width β, centered at $\omega = \omega_0$:

$$I(\omega) = N(A_0 V)^2 [B_0 L(D_T q^2) + B_2 L(D_T q^2 + 6D_R) + B_4 L(D_T q^2 + 20 D_R) + \cdots + B_{l_{\text{even}}} L(D_T q^2 + l(l+1) D_R) + \cdots] \qquad (28)$$

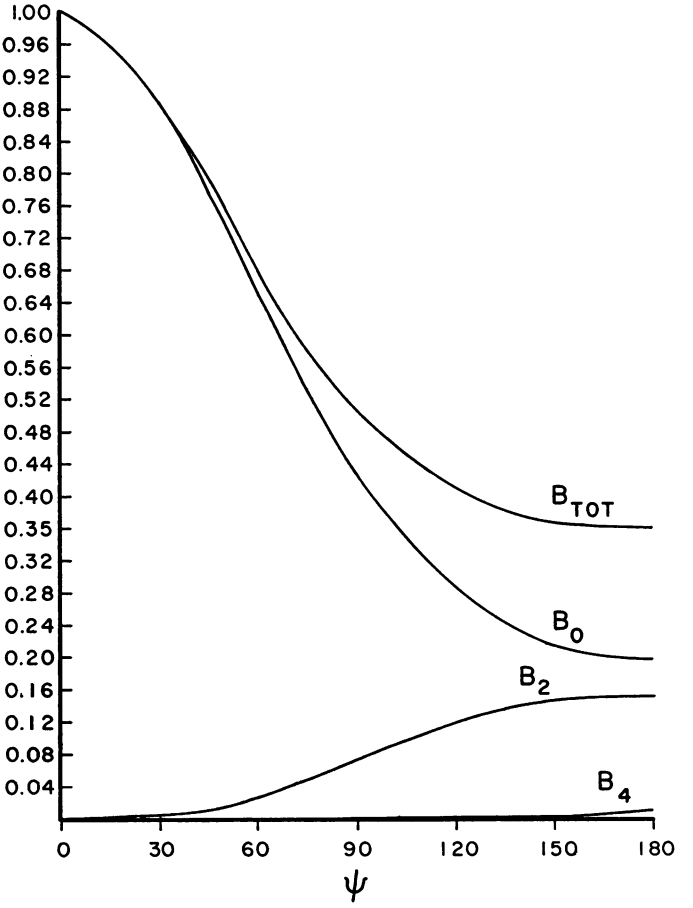

FIGURE 3 Plot of B_0, B_2, B_4, and B_{TOT} against scattering angle ψ for 3000 A long rods in water and with 6328 A incident light.

Thus the spectrum consists of a series of Lorentzians. The leading term is a Lorentzian of half-width $\Delta\omega_{\frac{1}{2}} = D_T q^2$, and is thus the "spherical" part of the spectrum. Its coefficient $N(A_0V)^2B_0$ is just the coefficient of the "spherical" part of Equation 25.

The additional terms depend on both translational *and* rotational diffusion. The combined intensities in all the terms for $l \geqq 2$ is:

$$I(\text{modified}) = N(A_0V)^2 \sum_{\substack{l=2 \\ \text{even}}}^{\infty} B_l$$

and must add up to the "modified" part of Equation 25. The complete spectrum is given by Equation 28 in terms of an infinite sum of Lorentzians.

In practice, the successive coefficients decrease rapidly enough so that the spectrum can be reasonably approximated by the first two or three terms.

In Fig. 3 we plot the coefficients B_0, B_2, and B_4 vs scattering angle ψ for 3000 A long rods in water ($n_0 = 1.33$) and with 6328 A incident light. In the same figure we show the normalized total intensity $I(\text{total})/N(A_0V)^2 = B_{\text{tot}}$. The dependence of B_{tot} on angle is used in the traditional angular intensity experiments, and was employed in an early study of TMV by Oster (2). Note that at small angles $B_0 \cong B_{\text{tot}}$ as expected. (Compare with Pecora, Fig. 1[8]). Also note that B_4 is negligible at all angles so that B_0 and B_2 determine the entire spectrum. Equation 28 can be used to predict the spectrum of light scattered by any rod-shaped scatterer once the coefficients B_l are known. The B_l can be readily evaluated from Equation 26 *b* in terms of $h = qL/2$. We have prepared tables of B_0, B_2, B_4, and B_{tot} for values of h at different scattering angles ψ in terms of n_0L/λ where n_0 is the refractive index of the solvent, L = the length of the scatterer, and λ is the vacuum wavelength of the incident light. These tables are available on request.

II. SPECTROSCOPIC TECHNIQUES

In part I we found that the spectrum of light scattered from a dilute solution of macromolecules consists of a series of Lorentzian components centered at ω_0, the frequency of the incident light (Equation 28). The width $\Delta\omega_{\frac{1}{2}}$ of the Lorentzian components is typically $\sim 3 \times 10^3$ Hz, while ω_0, the frequency of the incident light is $\sim 3 \times 10^{15}$ Hz. Thus direct measurement of the optical spectrum would require resolving powers in excess of 10^{12}, many orders of magnitude higher than the resolving powers of the best existing spectroscopic instruments.

Fortunately, there exists a technique which is ideally suited to the measurement of very narrow spectral lines. The technique utilizes the phenomenon of "optical beats" first observed by Forrester et al. in 1954 (13). The application of optical beating to the measurement of narrow spectral lines was subsequently discussed by Forrester (14). The basic concept of the method is that the intensity of the optical field at the detector (photomultiplier) fluctuates in time, and that the fluctuations become slower as the optical field becomes more nearly monochromatic. Since the photoelectric emission rate is proportional to the optical intensity, the photocurrent will fluctuate as the intensity fluctuates. Therefore, a measurement of the spectrum of the fluctuations of the photocurrent can be used to determine the spectral profile of the optical signal. For spectral lines with widths of several KHz, it is thus only necessary to measure the fluctuations in the photocurrent in the KHz range.

Glauber has derived the equations describing the light beating effect in a fully quantum mechanical development (15–17). We will present a similar but somewhat simpler analysis in which the optical field is treated as a classical variable, a procedure which is permissible for the type of optical fields we will consider here (18). In our discussion we will assume that the scattering volume is too small to be resolved by the collection optics so that the optical field is spatially coherent over

the photodector. The optical field is described by a real electric field vector $E_R\hat{e}$ where $\hat{e}$ is the unit polarization vector. $E_R(t)$ is represented as a fourier integral

$$E_R(t) = \int_{-\infty}^{\infty} v(\omega)e^{-i\omega t}\, d\omega$$

and we then define the complex analytical signal $E(t)$ (19) as the positive frequency part of $E_R(t)$:

$$E(t) = \int_{0}^{\infty} v(\omega)e^{-i\omega t}\, d\omega$$

(For a monochromatic field, $E_R(t) = 2E_0 \cos \omega t$ while $E(t) = E_0\, e^{-i\omega t}$).

The instantaneous intensity is defined to be $I(t) = E^*(t)E(t)$. The probability (per unit time) that a photoelectron will be emitted is:

$$W^{(1)}(t) = \beta I(t) = \beta E^*(t)E(t) \tag{29}$$

where β is a suitably defined quantum efficiency. The photoelectric current $i(t) = eW^{(1)}(t) = e\beta E^*(t)E(t)$ while the joint probability that one photoelectron will be emitted at time t (per unit time) and another at time $t + \tau$ (per unit time) is

$$W^{(2)}(t, t + \tau) = \beta^2 E^*(t)E(t)E^*(t + \tau)E(t + \tau) \tag{30}$$

We also will need the averages of $i(t)$ and $W^{(2)}(t, t + \tau)$ which for stationary fields are:

$$\langle i(t)\rangle = e\langle W^{(1)}(t)\rangle = e\beta\langle E^*(t)E(t)\rangle = e\beta\langle I\rangle$$

$$\langle W^{(2)}(t, t + \tau)\rangle = \beta^2\langle E^*(t)E(t)E^*(t + \tau)E(t + \tau)\rangle = \beta^2\langle I\rangle^2 g^{(2)}(\tau) \tag{31}$$

where

$$g^{(2)}(\tau) = \frac{\langle E^*(t)E(t)E^*(t + \tau)E(t + \tau)\rangle}{\langle E^*E\rangle^2}$$

The power spectrum $P_i(\omega)$ of the photocurrent is given by the Wiener-Khintchine theorem:

$$P_i(\omega) = \frac{1}{2\pi}\int_{-\infty}^{+\infty} e^{i\omega\tau}C_i(\tau)\, d\tau \tag{32}$$

where the current autocorrelation function is

$$C_i(\tau) = \langle i(t)i(t + \tau)\rangle = e^2\langle W^{(1)}(t)W^{(1)}(t + \tau)\rangle \tag{33}$$

(For distributed spectra centered at $\omega = 0$, Equation 32 is multiplied by 2 for $\omega > 0$, and set $= 0$ for $\omega < 0$). Now the photocurrent $i(t)$ actually consists of a series of discrete pulses which we will assume to be infinitely narrow. Therefore $C_i(\tau)$ has

two distinct contributions: If the electrons at t and $t + \tau$ are distinct,

$$\langle W^{(1)}(t)W^{(1)}(t + \tau)\rangle = \langle W^{(2)}(t, t + \tau)\rangle = \beta^2\langle I\rangle^2 g^{(2)}(\tau)$$

while if the *same* electron occurs at t and $t + \tau$,

$$\langle W^{(1)}(t)W^{(1)}(t + \tau)\rangle = \langle W^{(1)}(t)\rangle\delta(\tau) = \beta\langle I\rangle\delta(\tau)$$

Therefore,

$$C_i(\tau) = e^2\beta\langle I\rangle\delta(\tau) + e^2\beta^2\langle I\rangle^2 g^{(2)}(\tau)$$

$$C_i(\tau) = e\langle i\rangle\delta(\tau) + \langle i\rangle^2 g^{(2)}(\tau) \tag{34}$$

We consider below two different detection schemes which were analyzed from a different point of view by Forrester (14).

Case 1: Homodyne Detection

The homodyne detection scheme in which only the scattered light falls on the photodetector was first utilized by Ford and Benedek (20) in a study of critical opalescence, and was employed in the macromolecular scattering experiments of references 10 and 11.

Suppose the optical field is a narrow band Gaussian random field. (For coherent laser-light scattered by a dilute solution of scatterers, the Gaussian nature of the scattered field follows from the central limit theorem.)

The scattered field is characterized by an autocorrelation function

$$C_E(\tau) = \langle E^*(t)E(t + \tau)\rangle = \langle I\rangle g^{(1)}(\tau)$$

For Gaussian fields, the second-order correlation function $g^{(2)}(\tau)$ is related to $g^{(1)}(\tau)$ by (reference 18):

$$g^{(2)}(\tau) = 1 + |\, g^{(1)}(\tau)\,|^2 \tag{35}$$

whence

$$C_i(\tau) = e\langle i\rangle\delta(\tau) + \langle i\rangle^2(1 + |\, g^{(1)}(\tau)\,|^2) \tag{36}$$

In section I, we found that the autocorrelation function for the light scattered by rod-shaped scatterers underoing simultaneous rotational and translational diffusion is:

$$\langle E^*(t)E(t + \tau)\rangle = N(A_0V)^2\{e^{-i\omega_0\tau}\sum_{\substack{l=0\\ \text{even}}}^{\infty} B_l e^{-[D_T q^2 + l(l+1)D_R]\tau} \tag{37}$$

Thus $\langle I \rangle = N(A_0V)^2 \sum_l B_l$, and

$$g^{(1)}(\tau) = e^{-i\omega_0\tau} \sum_{\substack{l=0 \\ \text{even}}}^{\infty} B_l e^{-[D_T q^2 + l(l+1)D_R]\tau} / \sum_l B_l$$

$$= e^{-i\omega_0\tau} \sum_{\substack{l=0 \\ \text{even}}}^{\infty} B_l e^{-\Gamma_l \tau} / \sum_l B_l \qquad \text{(where } \Gamma_l = D_T q^2 + l(l+1)D_R\text{)}$$

If we keep only the two leading terms in $g^{(1)}(\tau)$, then

$$| g^{(1)}(\tau) |^2 \approx (B_0^2 e^{-2\Gamma_0\tau} + 2B_0B_2 e^{-(\Gamma_0+\Gamma_2)\tau} + B_2^2 e^{-2\Gamma_2\tau)} / (B_0 + B_2)^2$$

so that:

$$C_i(\tau) = e\langle i \rangle \delta(\tau) + \langle i \rangle^2 \left[1 + \frac{(B_0^2 e^{-2\Gamma_0\tau} + 2B_0B_2 e^{-(\Gamma_0+\Gamma_2)\tau} + B_2^2 e^{-2\Gamma_2\tau)}}{(B_0+B_2)^2} \right] \quad (38)$$

The spectrum of the photocurrent is then given by Equations 32 and 38:

$$P_i(\omega) = e \frac{\langle i \rangle}{\pi} + \langle i \rangle^2 \delta(\omega) + \frac{2\langle i \rangle^2}{(B_0 + B_2)^2}$$

$$\cdot \left\{ B_0^2 \frac{2\Gamma_0/\pi}{\omega^2 + 4\Gamma_0^2} + 2B_0B_2 \frac{(\Gamma_0 + \Gamma_2)/\pi}{\omega^2 + (\Gamma_0 + \Gamma_2)^2} + B_2^2 \frac{2\Gamma_2/\pi}{\omega^2 + 4\Gamma_2^2} \right. \quad (39)$$

Apart from a constant factor this result is the equivalent of that given by Glauber (17).

The first term in Equation 39 is the shot noise, and the second is a direct current component (which is blocked in a real experiment). The last three terms are Lorentzians centered at $\omega = 0$ which arose from the two Lorentzians (Γ_0, Γ_2) in the optical spectrum. The first and third Lorentzians have, respectively, just twice the width of the two components in the optical spectrum, while the second Lorentzian ($\Gamma_0 + \Gamma_2$) is a cross-term resulting from the beating of the two optical Lorentzians against each other in the square-law photodetection process.

The half-widths at half maximum of the three Lorentzian components in the photoelectric spectrum are:

$$\Delta\omega_{\frac{1}{2}} = 2D_T q^2$$

$$\Delta\omega_{\frac{1}{2}} = 2D_T q^2 + 6D_R$$

$$\Delta\omega_{\frac{1}{2}} = 2D_T q^2 + 12D_R \quad (40)$$

$P_s(0)$, the power in the leading Lorentzian ($2D_T q^2$) at zero frequency is

$$\frac{\langle i\rangle^2 B_0^2}{(B_0 + B_2)^2 \pi\Gamma_0} \cong \frac{\langle i\rangle^2}{\pi D_T q^2}$$

while $P_s(0)$ relative to the constant shot-noise background is the "signal to shot-noise ratio":

$$\frac{P_s(0)}{P_N} \cong \frac{\langle i\rangle^2}{D_T q^2 e\langle i\rangle} = \frac{\langle i\rangle}{eD_T q^2} \tag{41}$$

which is the mean photoelectron emission rate divided by the optical linewidth.

Case 2. Heterodyne Detection

In case 1, we considered the spectrum of the photocurrent with the detector illuminated by light scattered by the macromolecules. As an alternative procedure, the detector can be illuminated simultaneously by the scattered light and by a coherent local oscillator signal. This heterodyne detection scheme was utilized in the original polystyrene experiment of Cummins, Knable, and Yeh (9) and was extended to the study of critical opalescence by Alpert and coworkers (21, 22).

In the experiments described in this paper, the local oscillator signal was produced by placing a stationary object within the scattering volume so that the scattered field and the local oscillator field were spatially coherent. Also, the frequency of the local oscillator signal is ω_0, the center frequency of the scattered spectrum.

Let the scattered light field be E_s and the local oscillator field be E_{LO}. The photocurrent produced by either E_s or E_{LO} in the absence of the other is i_s or i_{LO} where

$$\langle i_s(t)\rangle = e\beta\langle E_s^*(t)E_s(t)\rangle$$

$$\langle i_{LO}(t)\rangle = e\beta\langle E_{LO}^*(t)E_{LO}(t)\rangle = e\beta|E_{LO}|^2 \tag{42}$$

since $|E_{LO}|^2$ is constant.

The current autocorrelation function

$$C_i(\tau) = e^2\beta\delta(\tau)\langle E^*(t)E(t)\rangle + e^2\beta^2\langle E^*(t)E(t)E^*(t+\tau)E(t+\tau)\rangle$$

simplifies considerably if the local oscillator field is much stronger than the scattered field so that $i_{LO} \gg i_s$. When $\langle E^*(t)E(t)E^*(t+\tau)E(t+\tau)\rangle$ is expanded using $E(t) = E_s(t) + E_{LO}(t)$, the result contains 16 terms of which 10 are zero, and three are time independent terms whose sum is $L_{LO}^2 + 2I_{LO}\langle I_s\rangle$. The remaining three terms give

$$I_{LO}\{e^{+i\omega_0\tau}\langle E_s^*(t)E_s(t+\tau)\rangle + e^{-i\omega_0\tau}\langle E_s(t)E_s^*(t+\tau)\rangle\} + \langle E_s^*(t)E_s(t)E_s^*(t+\tau)E_s(t+\tau)\rangle$$

If $I_{LO} \gg \langle I_s\rangle$, we can neglect the last term in the preceding line and also keep only

I_{LO}^2 of the D.C. terms. Thus

$$C_i(\tau) = e^2\beta I_{LO}\delta(\tau) + e^2\beta^2 I_{LO}^2 + e^2\beta^2 I_{LO}\langle I_s\rangle \cdot (e^{+i\omega_0\tau} g_s^{(1)}(\tau) + e^{-i\omega_0\tau} g_s^{(1)*}(\tau)) \tag{43}$$

now from Equation 37

$$g_s^{(1)}(\tau) = e^{-i\omega_0\tau} \sum_{\substack{l=0 \\ \text{even}}}^{\infty} B_l e^{-\Gamma l\tau} \Big/ \sum_{\substack{l=0 \\ \text{even}}}^{\infty} B_l$$

$$C_i(\tau) = ei_{LO}\delta(\tau) + i_{LO}^2 + 2i_{LO}\langle i_s\rangle \sum_{\substack{l=0 \\ \text{even}}}^{\infty} B_l e^{-\Gamma l\tau} \Big/ \sum_{\substack{l=0 \\ \text{even}}}^{\infty} B_l \tag{44}$$

so that the photocurrent power spectrum is

$$P_i(\omega) = \frac{ei_{LO}}{\pi} + i_{LO}^2\delta(\omega) + 4i_{LO}\langle i_s\rangle \sum_{\substack{l=0 \\ \text{even}}}^{\infty} B \frac{\Gamma_l/\pi}{l\omega^2+\Gamma_l^2} \Big/ \sum_{\substack{l=0 \\ \text{even}}}^{\infty} B_l \tag{45}$$

Again the first term is the shot noise and the second is a direct current signal which can be blocked.

The last term consists of a sum of Lorentzians centered at $\omega = 0$, one for each Lorentzian in the optical spectrum. Notice that the photocurrent Lorentzians have the *same* width as the optical Lorentzians (rather than twice the width as in the homodyne case) and that there are *no cross terms*. This is the result of having the scattered field beat against the local oscillator which has also removed the necessity of stipulating that the optical field have Gaussian statistics.

Finally, note that the power at $\omega = 0$ in the leading Lorentzian relative to the shot noise is

$$\frac{P_s(0)}{P_N} = \frac{4i_{LO}\langle i_s\rangle\pi}{\pi D_T q^2 e i_{LO}} = \frac{4\langle i_s\rangle}{eD_T q^2} \tag{46}$$

which is four times larger than in the homodyne case (Equation 41).

III. INSTRUMENTATION

Apparatus. A schematic diagram of the spectrometer utilized in our experiments is shown in Fig. 4. Plane-polarized, monochromatic ($\lambda = 6328$ A) light produced by a Spectra-physics (Spectra-Physics, Inc., Mountain View, Calif.) model 125 He-Ne laser was focused by a thin lens on the sample contained in a cuvette. Light scattered at an angle ψ to the forward direction, $\mathbf{K}_0$, was collected and imaged on a variable aperture located at the face of the photomultiplier. An adjustable aperture located at the focal point of the first collimating lens was used to control the angular

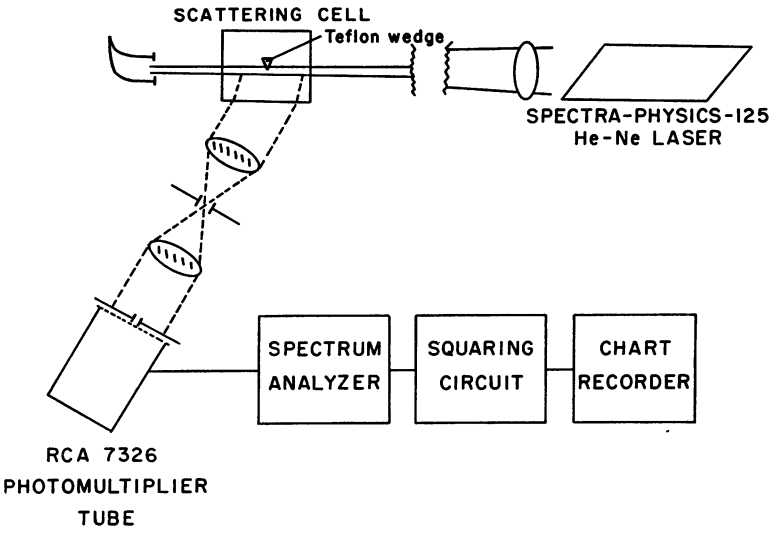

FIGURE 4 Schematic diagram of the spectrometer showing teflon wedge in heterodyne configuration.

acceptance, $\Delta\psi/\psi$, of the collecting system. In the experiments reported here $\Delta\psi/\psi <$ 0.015. An RCA 7326 photomultiplier was used as a detector. The aperture in front of the photomultiplier served to limit the extent of the area of the active surface of the photomultiplier that was illuminated by the image of the scattering sample and its diameter was selected to give optimal signal to noise ratios.

The power spectral density of the photomultiplier current was measured by squaring and averaging the output of a Tektronix 1L5 spectrum analyzer (Tektronix, Inc., Beaverton, Ore.) and recording the final output on a strip chart recorder. A single power spectral density determination could be made in a minute or so and a spectrum of ten to fifteen points took 15–20 min to record. During this time the laser power showed drifts of less than a few tenths of a per cent.

Calibration and Shot-Noise Determination. A shot-noise source consisting of a battery-powered flash light bulb with an adjustable intensity was utilized in order to check both the uniformity of frequency response and the linearity of the over-all system (photomultiplier, amplifiers, spectrum analyzer, and recorder). The frequency response was flat from 50 Hz to 0. 1 MHz. Linearity in power was checked by verifying that shot noise power varied linearly with photomultiplier current. The over-all system showed a stable, reproducible, response linear with average photomultiplier current to better than 2% of the full scale deflection of the strip chart recorder.

The flash light bulb source was used also as a substitute source to determine the shot noise power in the signal. The power spectral density of a sample was measured

and the average photomultiplier current was noted. The laser beam was then blocked, and the intensity of the flash light bulb was adjusted to give an average photomultiplier current equal to that produced by the scattered light. The shot-noise power for this value of photomultiplier current was measured on the spectrum analyzer and taken to be equal to the shot noise power present in the photomultiplier current power spectrum, in the presence of the signal from the sample. Accordingly, it was subtracted from the total power spectrum to obtain the power spectral density of the photomultiplier current that was due to the light beating signal or "excess photon noise" in the light scattered by the sample.

Homodyne and Heterodyne Spectra. As shown in section II an optical signal consisting of two Lorentzians is transformed on homodyning at a photomultiplier into a power spectrum that consists of the sum of three Lorentzians, plus a flat shot-noise spectrum. The shot noise is easily determined as described above, but the presence of a third Lorentzian in the spectrum complicates the data analysis and severely restricts the usefulness of the method. The heterodyning technique, also discussed in section II does not introduce a third Lorentzian into the power spectrum and has the added advantage of increasing the signal to noise ratio by a actor of 4.

Bergé and Volochine introduced a plate of appropriately cut smoky quartz into the sample cuvette as a source of stationary scatterers to serve as a local light source or oscillator that would heterodyne with the light scattered from the diffusing scatterers.[2] Light scattered from fixed microscopic inclusions in the smoky quartz experiences no spectral shift and serves as a local heterodyne oscillator that optically mixes with the spectrally shifted light scattered from diffusing particles that are close to the surface of the quartz plate. We tried smoky quartz and found that it did not scatter sufficiently uniformly at all angles to make it generally useful. We have made "local oscillators" by embedding small polystyrene spheres in the surface of a lucite plate. These showed more uniform scattering and worked satisfactorily but were difficult to keep clean when used with protein solutions. The most successful local oscillator that we have developed so far consists of a small prism of teflon of triangular cross section. The prism was positioned so that one of its edges partially interrupted the main beam in that region of the sample that was imaged on the photomultiplier. The heterodyne results reported below were obtained in this way.

We have encountered some difficulty with the heterodyning technique due to movement of the teflon prism relative to the solution of scatterers. Such movement produces a spurious signal that contributes to the power spectrum. Building vibrations that disturb the sample are troublesome particularly at low frequencies. At the time of these studies our spectrometer was not completely isolated from me-

[2] Bergé, P. Communication presented at the meeting of the French Crystallographic Society. Apri 1967. Unpublished.

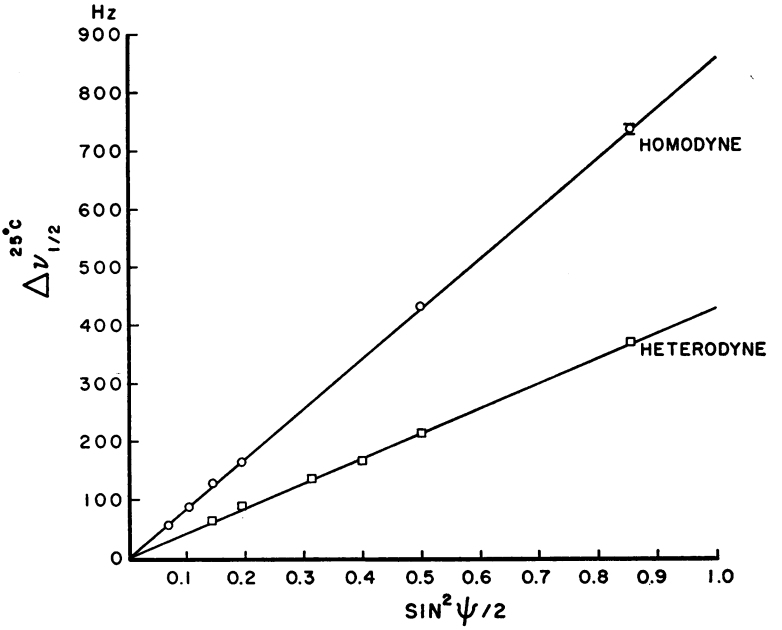

FIGURE 5 Single Lorentzian half-widths at 25°C as a function of $\sin^2\psi/2$ obtained from homodyne and heterodyne spectra of polystyrene latex spheres, 0.126 ± 0.004 μ diameter, 0.01 mg/ml; ○, homodyne spectra; □, heterodyne spectra.

chanical disturbances and we believe that our heterodyne measurements below a hundred cycles are less reliable on this account.

As a check on the operational characteristics of the spectrometer, homodyne spectra were recorded for polystyrene latex spheres of diameter 0.126 ± 0.004 μ and fitted to single Lorentzians. Half-widths of spectra varied linearly with q^2/π (see Fig. 5) as expected for isotropic particles whose rotation cannot affect the spectrum of scattered light. A linear least-squares fit of half-width against q^2/π, reduced to 20°C, gave a slope corresponding to a translational diffusion constant, of $D_T^{20°} = 0.341 \pm 0.005 \times 10^{-7}$ cm²/sec. The value for the translational diffusion constant of these spheres as calculated from the known dimensions of the spheres and the Stokes-Einstein relationship (23) for the diffusion constant was $D_T^{20°} = 0.338 \pm 0.010 \times 10^{-7}$ cm²/sec.

Polystyrene latex spheres (PSL), were obtained from the Dow Chemical Co., Midland, Mich. Suspensions containing spheres at a concentration of 0.01 mg/ml were made up in an aqueous solution of 0.01% sodium lauryl sulfate. When not in use these suspensions were stored at 2°C. They showed little or no tendency to aggregate over periods of several weeks and their light scattering behavior conformed very closely to theoretical expectations for a monodisperse system of spherical scatterers. They were on this account useful as a test sample for periodically checking the absolute accuracy and stability of the spectrometer.

IV. RESULTS

Tobacco Mosaic Virus. Since our major experimental objective was to check the validity of the theory of spectral broadening on light scattering from a solution of identical rod-like scatterers it was imperative that any test specimen used for this purpose be monodisperse. Tobacco mosaic virus particles (TMV) have a length of 3000 ± 50 A and a diameter of 180 A according to X-ray diffraction, electron microscopy, and physical chemical studies (24–27). Light scattering, flow birefringence, viscosity, sedimentation, and diffusion studies on TMV have established that at low ionic strengths and a pH above 7.3–7.5 dilute, stable, monodisperse solutions of TMV do exist and further that they show no evidencc of monomer-polymer equilibria (24). O'Konski and Haltner found that monodisperse preparations of TMV in 0.001 M phosphate at pH 7 that were initially monodisperse showed no dimer formation over a 2 year period (28). They also found that initially polydisperse preparations with the same concentration of virus particles showed different amounts of monomer and dimer present. From these results they concluded that a monomer-dimer equilibrium situation does not exist in dilute solutions of TMV and that the presence of dimer particles had to be attributed to uncontrolled variables in the process of preparation or to a property of the biological system.

In view of these facts we believe that TMV in dilute solutions of low ionic strength and pH 7.5 can be regarded as a highly monodisperse suspension of rigid rods of uniform length and diameter. Consequently, any deviation of the light scattering behavior of such solutions from that predicted by the theory developed for monodisperse systems cannot be attributed to polydispersity.

Steere and Ackers and Steere have described procedures for preparing and keeping highly monodisperse suspension of tobacco mosaic virus (TMV) particles in aqueous solutions (29, 30). The TMV preparations used in this work were prepared and fractionated by Dr. Steere in his laboratory and were assayed by him for monodispersity by direct electron microscopic observation. The TMV particles were suspended in 0.001 M sodium phosphate buffer, pH 7.5, at a concentration of 0.1 mg/ml. Electron microscope assays of the samples showed virtually no short pieces of virus particles or aggregates. Electron microscopic assay after exposure to the laser beam for spectral measurements also showed no pieces of virus particles or aggregates. Furthermore, repeat spectra on the same sample showed good agreement and the power spectral density did not depend on the beam intensity. Exposure to the laser beam did not therefore produce any appreciable polydispersity in the sample.

All experiments were done at room temperature (20°–25°C) and diffusion constants have been reduced to 20°C after corrections for the temperature dependence of the viscosity of water.

Standard errors were computed using Student's t-distribution with 70% confidence limits.

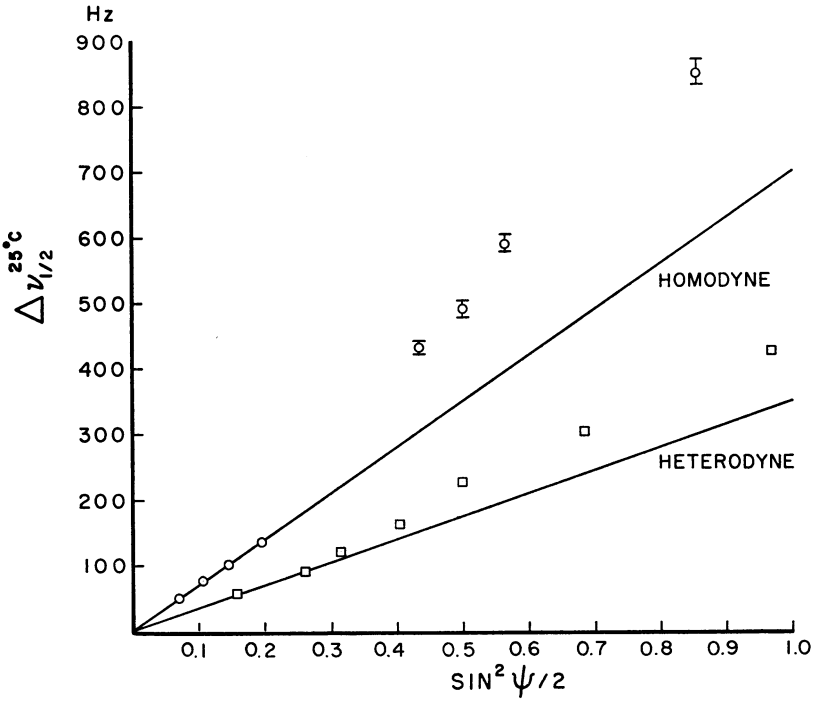

FIGURE 6 Single Lorentzian half-widths at 25°C as a function of $\sin^2\psi/2$ obtained from homodyne and heterodyne spectra of TMV; ○, homodyne spectra; □, heterodyne spectra; solid lines correspond to best-least squares linear fit to data for $\psi < 60°$.

TMV Homodyne Spectra. Homodyne spectra of TMV solutions were recorded at various scattering angles ranging from 20° to 120°. At each angle four to ten power spectra were measured. A single power spectrum was obtained by making power measurements at ten to fifteen discrete frequencies ranging from about one-fifth the frequency of half maximum power to three to four times that frequency. Each spectrum was fitted to a single Lorentzian by a best-least squares procedure and the fitted half-widths were averaged. A plot of the half-widths of these single Lorentzians against $\sin^2\psi/2$ is shown in Fig. 6. Unlike the polystyrene latex spheres, TMV Rayleigh linewidths do not show a simple linear dependence on $\sin^2\psi/2$ if a single Lorentzian power spectral density function is assumed. Since we know in this case that we are dealing with a monodisperse solution of TMV particles the observed systematic departure from linearity cannot be attributed to polydispersity. Its explanation must be sought in some other property of the scatterers.

TMV Heterodyne Spectra. Heterodyne spectra were also taken on TMV solutions in much the same way that the homodyne spectra were obtained except that a teflon wedge was used to introduce a local oscillator signal as described

above, and spectra were recorded for scattering angles ranging from about 45° to 160°. Here again each spectrum was fitted to a single Lorentzian and the half-widths plotted against $\sin^2 \psi/2$, see Fig. 6. The heterodyne spectra have half-widths that are about one-half those of the corresponding homodyne spectra in accord with the theory of section II, but they too deviate systematically from a linear dependence on $\sin^2 \psi/2$.

Double-Lorentzian Analysis of Spectra. As shown in section II the homodyne spectra of rod-like scatterers, after removal of the D.C. and shot-noise terms, consists of the sum of three Lorentzians, all centered at zero frequency (see Equation 39). For rods having the dimensions of TMV particles only the first Lorentzian in equation 39 is significant for $\psi < 60°$. For $60° < \psi < 120°$ the first Lorentzian and the second Lorentzian are significant and for $120° < \psi$, the third Lorentzian becomes significant also.

Heterodyne spectra of TMV however, are closely approximated by two Lorentzians at all scattering angles. For heterodyne spectra obtained from TMV particles only the first Lorentzian is significant for $\psi < 60°$ and the second becomes appreciable for $100° < \psi$.

On this basis, it is to be expected that homodyne spectra for $\psi < 120°$ degrees and heterodyne spectra for all ψ should resolve into two Lorentzians centered at zero frequency. For homodyne spectra, $\psi < 120°$, the two significant Lorentzians have half-widths of $2q^2D_T$ and $(2q^2D_T + 6D_R)$ respectively. For heterodyne spectra at all angles the half-widths are q^2D_T and $(q^2D_T + 6D_R)$. In both cases, in the limit of zero scattering angle, the second Lorentzian is negligible and the spectra are single Lorentzians whose half-widths vary directly with $\sin^2\psi/2$. Accordingly, the single Lorentzian analysis of TMV spectra obtained for $\psi < 60°$ should permit an estimate of D_T. Homodyne spectra obtained for $60° < \psi < 120°$ and heterodyne spectra for $\psi > 60°$ should consist of two Lorentzians, and a determination of the half-widths of the second Lorentzian from such spectra, together with a knowledge of the half-widths of the first Lorentzian enables one to estimate D_R directly.

Double Lorentzian fits for all spectra were obtained as follows. First for $\psi < 60°$ single Lorentzian best-least squares fits were made under the constraint that the half-widths should show a linear dependence on $\sin^2 \psi/2$. These gave half-widths of $705 \sin^2 \psi/2$ Hz for homodyne spectra and $353 \sin^2 \psi/2$ Hz for heterodyne spectra corresponding in both cases to a translational diffusion coefficient, D_T, reduced to 20°C of $0.280 \pm 0.006 \times 10^{-7}$ cm²/sec. The solid lines shown in Fig. 6 indicate the dependence of the half-width of this single "translational" Lorentzian on $\sin^2 \psi/2$.

Using the value of D_T obtained from single Lorentzian fits for $\psi < 60°$, two Lorentzian fits were obtained for $\psi > 60°$ by a best-least squares procedure under the constraint that the half width of one of the fitted Lorentzians have $\Gamma_0' = 2q^2D_T$

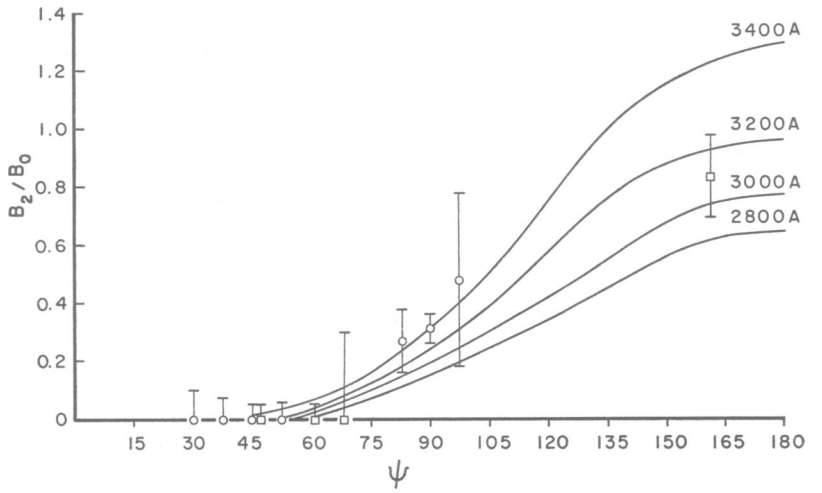

FIGURE 7 Plot of B_2/B_0 obtained from best double-Lorentzian fits to homodyne spectra (○) and heterodyne spectra (□) squares. Solid curves were derived from Table I (A and B) for particles with the lengths indicated.

for homodyne spectra and $\Gamma_0 = q^2D_T$ for heterodyne spectra. In the case of the homodyne spectra this fitting procedure yielded a half width of $\Gamma_2' = 2q^2D_T + 6D_R$ for the second Lorentzian and the relative powers B_0 and B_2 of the two Lorentzians. Subtraction of $2q^2D_T$ from Γ_2' yielded values for $6D_R$. For the heterodyne spectra Γ_0 was constrained to be q^2D_T (half that of the homodyne spectra) and $\Gamma_2 = q^2D_T + 6D_R$ as well as the relative powers B_0 and B_2 were obtained from the two Lorentzian fit.

For homodyne spectra at scattering angles corresponding to $\sin^2 \psi/2 = 0.435$, 0.500, and 0.575 and for heterodyne spectra at a scattering angle corresponding to $\sin^2 \psi/2 = 0.970$, the double-Lorentzian fitting procedure produced two Lorentzians the sum of which gave a significantly better fit to the data than the best single Lorentzian fit. In this sense the spectra at these angles were "resolved" into their two Lorentzian components. The homodyne spectra at $\sin^2 \psi/2 = 0.856$ and the heterodyne spectra at $\sin^2 \psi/2 = 0.685$, 0.500, and 0.404 did not produce a two-Lorentzian fit that was any better than the single Lorentzian fit even though their best single Lorentzian fits departed from linearity. In this sense these spectra were not resolved into their two component Lorentzians. This does not mean, however, that these spectra do not consist of two Lorentzians but rather than the intrinsic errors in the power spectra are of sufficient magnitude to override any improvement in fit that the two Lorentzian procedure might have produced.

Refinement of Double-Lorentzian Fit. Using the double-Lorentzian parameters obtained in those instances where the spectra were resolved by the initial double-Lorentzian fit, a refinement was added to the fitting procedure in order to

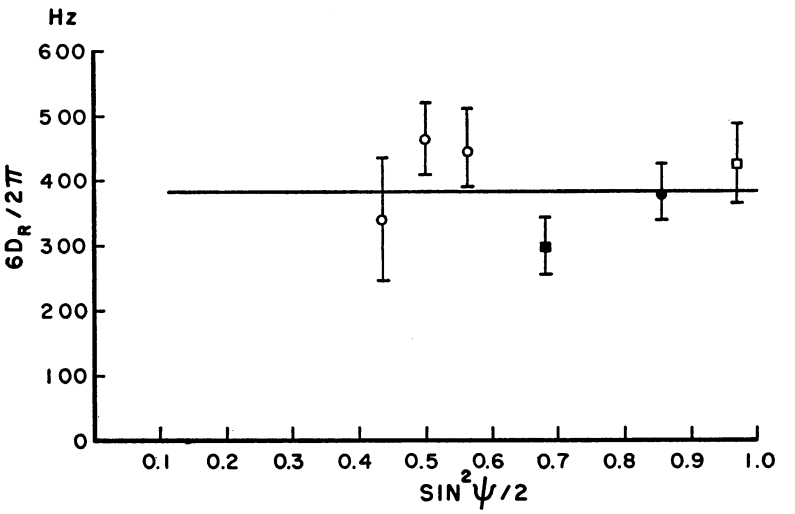

FIGURE 8 Plot of $6D_R/2\pi$, at 25°C, against $\sin^2\psi/2$; ○, homodyne spectra; □, heterodyne spectra. Open points indicate values derived from initial double Lorentzian fit; filled points from refined double Lorentzian fit.

resolve those spectra which were initially unresolved. Using the parameters obtained from the resolved spectra a plot of the ratio of the relative powers, B_2/B_o against ψ was made. This plot is shown in Fig. 7. Comparison of these data with the values of the power ratios derived from the Rayleigh-Gans theory of section I showed that the data conform best to those B_2/B_0 values that would be found for a rod-like scatterer 3200 ± 200 A in length. Using this additional information a second double Lorentzian fit was made on these unresolved spectra under the *additional* constraint that the ratio of the relative powers of the two Lorentzians be that given by a 3200 A rod at the corresponding scattering angle. This refined fitting procedure resolved the homodyne spectra for $\sin^2\psi/2 = 0.855$ and the heterodyne spectra for $\sin^2\psi/2 = 0.683$ into two Lorentzians in the sense that there was a clearly discernible small range of values of the half-width of the second Lorentzian which gave a resultant linewidth that corresponded closely to the experimentally observed value and at the same time was compatible with the values of B_2/B_0 expected from a rod-like particle 3200 ± 200 A in length.

Fig. 8 is a plot of the values of $6D_R/2\pi$ derived from both homodyne and heterodyne spectra including those values of the half-width obtained by means of the initial double Lorentzian fit and the refined double Lorentzian fit. The refinement procedure did not lead to a resolution of the heterodyne spectra for values of $\sin^2\psi/2 < 0.5$ even though these spectra gave rise to single Lorentzian fits that departed significantly from linearity. The average value for $6D_R/2\pi$ obtained from the half-width of the second Lorentzian at 25°C was 384 ± 22 Hz. This value

corresponds to a rotational diffusion coefficient, D_R, reduced to 20°C of 320. ± 18. sec^{-1}.

V. DISCUSSION

The experiments reported here were undertaken in order to resolve the translational and rotational diffusion broadening components of the Rayleigh line of TMV particles and to extract from the results estimates of the translational and rotational diffusion constants of these particles. Our results together with experimental values from the literature and values calculated from various hydrodynamic models are given in Table I. Our value for the rotational diffusion coefficient is in good agreement with O'Konski's which was obtained from transient electric birefringence measurements. Both of these experimental values seem compatible with calculated values obtained from the Burgers, Broersma, or Filson hydrodynamic models.

TABLE I

A. TRANSLATIONAL DIFFUSION CONSTANTS OF TMV

$D_T^{20^\circ} \times 10^7$ (cm^2/sec)

Experimental		Calculated (rod 3000 A × 180 A diameter)	
Rayleigh linewidth	0.280 ± 0.006	Perrin equations¶	0.502
Triebel‡	0.475 ± 0.012	Perrin equations, equivalent volume**	0.472
Dubin et al.*§	0.350 ± 0.020	Burgers equations‡‡	0.486
		Broersma equations‡‡	0.396
		Bloomfield shell models‡‡	0.480

B. ROTATIONAL DIFFUSION CONSTANTS OF TMV

$D_R^{20^\circ}$ (sec^{-1})

Experimental		Calculated (rod 3000 A × 180 A diameter)	
Rayleigh linewidth	320. ± 18.	Perrin equations¶	429.
O'Konski*‖	292. ± 6.	Perrin equations, equivalent volume**	402.
		Burgers equations*§§	385.
		Broersma equations*§§	276.
		Filson shell models*§§	349.

* Reduced from 25°C using temperature and viscosity dependence of Perrin equations, reference 23.

‡ Reference 32.

§ Reference 10.

‖ Reference 28.

¶ Reference 23, ellipsoid with axes a = 3000 A, b = 180 A.

** Reference 23, ellipsoid with length a = 3000 A, but axial ratio giving the same volume as for a 3000 A × 180 A diameter cylinder.

‡‡ Calculated from frictional radii given by Bloomfield, V. A., K. E. Van Holde, and W. O. Dalton. 1967. *Biopolymers* **5**: 149.

§§ Filson, O. P., and V. A. Bloomfield. 1967. *Biochemistry* **6**: 1650.

The translational diffusion coefficient found here is significantly lower than other reported values. The value cited by Dubin et al. was obtained from Rayleigh linewidth measurements identical to ours on a sample of TMV whose monodispersity had not been checked (10). These authors experienced difficulties in obtaining good single Lorentzian fits to their data. The value for D_T which they report, $0.350 \pm 0.020 \times 10^{-7}$ cm²/sec, was obtained from a best single Lorentzian fit to the spectra obtained at a scattering angle of 90°. They do not report any estimates for D_T based on spectra taken at smaller scattering angles. Presumably their data would have given a plot of half width against $\sin^2 \psi/2$ that deviated from linearity with $\sin^2 \psi/2$ in a manner similar to our data along a curve that is concave upward, see Fig. 6. If such were the case an estimate of D_T obtained from the limiting slope as ψ approaches zero would have been smaller than 0.350×10^{-7} cm²/sec, the figure which they reported. A single Lorentzian fit to our data obtained at 90° yields a value of $0.386 \pm 0.14 \times 10^{-7}$ cm²/sec for D_T which is considerably larger than the value $0.280 \pm 0.006 \times 10^{-7}$ cm²/sec, obtained in the limit of zero scattering angle. The difference between our value for D_T and that obtained by Dubin et al., could very likely be due to the fact that their estimate was not obtained in the limit of zero scattering angle.

The value of D_T given by Triebel et al. corresponds to D_T in the limit of zero concentrations of virus particles. It was obtained by extrapolating sedimentation measurements made on TMV suspended in 0.02 M phosphate buffer at various concentrations of virus particles down to 0.5 mg/ml (31). Our sample was at a much lower ionic strength, 0.001 M sodium phosphate, and concentration, 0.1 mg/ml. Since TMV carries a charge in the neighborhood of −2,000 at a pH of 7.5 it is quite possible that at the low ionic strength of our sample the effects of charge on the translational diffusion coefficient are appreciable, while at high ionic strengths they are reduced.

APPENDIX

The Phase Autocorrelation Function

The phase autocorrelation $C_\phi(\tau)$ is defined in Equation 10 as

$$[C_\phi(\tau)] = \langle e^{-i\mathbf{q}\cdot\mathbf{r}(t)} e^{i\mathbf{q}\cdot\mathbf{r}(t+\tau)} \rangle \tag{A-1}$$

which is the time average of the quantity $e^{-i\mathbf{q}\cdot\mathbf{r}(t)} e^{i\mathbf{q}\cdot\mathbf{r}(t+\tau)}$. Assuming the system to be ergodic we can equate this time average to an ensemble average:

$$\begin{aligned}[C_\phi(\tau)] &= \left\langle \int W^c(r_0, t \mid r_0 + R, t + \tau) e^{-i\mathbf{q}\cdot\mathbf{r}_0} e^{i\mathbf{q}\cdot(\mathbf{r}_0+\mathbf{R})}\, d^3R \right\rangle_{r_0} \\ &= \left\langle \int W^c(r_0, t \mid r_0 + R, t + \tau) e^{i\mathbf{q}\cdot\mathbf{R}}\, d^3R \right\rangle_{r_0} \end{aligned} \tag{A-2}$$

Where $W^c(r_0, t \mid r_0 + R, t + \tau)$ is the conditional probability that a scatterer located at

r_0 at time t will be in a unit volume at $r_0 + R$ at time $t + \tau$, and the angular brackets with a subscript r_0 mean an ensemble average over all r_0. Since the system is isotropic, homogeneous, and stationary, W^c cannot depend on r_0 or t. Therefore,

$$[C_\phi(\tau)] = \int G_s(\mathbf{R}, \tau) e^{i\mathbf{q}\cdot\mathbf{R}} d^3R \tag{A-3}$$

where $G_s(R, \tau)$, the ensemble averaged conditional probability that a particle located at the origin at time $t = 0$ will be (in a unit volume) at R at time τ, is the "self" part of the space-time correlation function of Van Hove (4) in the classical limit.

We consider three cases.

Case A: Fixed Scatterers

$$G_s(R, \tau) = \delta(R) \tag{A-4}$$

$$[C_\phi(\tau)] = \int \delta(R) e^{i\mathbf{q}\cdot\mathbf{R}} d^3R = 1 \tag{A-5}$$

Case B: Scatterers Moving with Fixed Velocity v

$$G_s(R, \tau) = \delta(\mathbf{R} - \mathbf{v}\tau) \tag{A-6}$$

$$[C_\phi(\tau)] = \int \delta(\mathbf{R} - \mathbf{v}\tau) e^{i\mathbf{q}\cdot\mathbf{R}} d^3R = e^{i\mathbf{q}\cdot\mathbf{v}\tau} \tag{A-7}$$

Case C: Diffusion

We consider scatterers undergoing continuous frequent collisions with the (small) solvent molecules. If we neglect very short times (comparable to the reciprocal of the collision frequency ω_c), the time evolution of G_s is determined by the macroscopic diffusion equation which describes the ensemble averaged behavior of the microscopic system. Hence:

$$\frac{\partial G_s}{\partial t} = D_T \nabla^2 G_s \tag{A-8}$$

where D_T is the translational diffusion constant.

The diffusion Equation A-8 can be solved directly with $G_s(\tau = 0) = \delta(R)$.

$$G_s(R, \tau) = \frac{1}{(4\pi D_T \tau)^{3/2}} e^{-R^2/4D_T\tau} \tag{A-9}$$

Combining A-3 and A-9,

$$[C_\phi(\tau)] = e^{-D_T q^2 \tau} \tag{A-10}$$

Equation A-10 can also be found directly from Equations A-3 and A-8 without solving for $G_s(R, \tau)$.

The eigenfunctions of the diffusion Equation A-8 are: $e^{i\mathbf{q}'\cdot\mathbf{R}}e^{-q'^2D_T\tau}$. Thus the integration in (A-3) picks out the $q' = q$ component of G_s and leaves, after integration

$$[C_\phi(\tau)] = e^{-D_T q^2 \tau}$$

It is a pleasure to acknowledge our gratitude to Dr. Russell L. Steere, Plant Virology Laboratory, Agriculture Research Service, U.S.D.A., Beltsville, Md. for providing us with the highly monodisperse preparations of TMV and for assaying our samples for monodispersity, both before and after use.

This research was supported by a grant from the U. S. Public Health Service (5-R01-HE-03141) to F. D. Carlson. A preliminary report of this work was given at the 12th Annual Meeting of the Biophysical Society, February 1968, Pittsburgh, Pa. (*Biophys. Soc. Annu. Meet. Abstr.* **2:** A-95. 1968).

T. J. Herbert is U. S. P. H. S.—Nat. Inst. of Gen. Med. Science Predoctoral Fellow (5-F1-GM-33,504).

G. Woods is U. S. P. H. S.—N. I. H. Training Grant Predoctoral Fellow (5-T01-GM716).

Received for publication 5 December 1968.

REFERENCES

1. DEBYE, P. 1947. *J. Phys. Colloid Chem.* **51**:18.
2. OSTER, G. 1948. *Chem. Rev.* **43**:319.
3. VAN DE HULST, H. C. 1957. Light Scattering by Small Particles. John Wiley & Sons, New York. Chapter 7.
4. VAN HOVE, L. 1954. *Phys. Rev.* **95**:249.
5. KOMAROV, L. I., and I. Z. FISHER. 1963. *Soviet Phys. JETP* **16**:1358.
6. PECORA, R. 1964. *J. Chem. Phys.* **40**:1604.
7. STEELE, W. A., and R. PECORA. 1965. *J. Chem. Phys.* **42**:1863; PECORA, R., and W. A. STEELE. 1965. *J. Chem. Phys.* **42**:1872; PECORA, R. 1965. *J. Chem. Phys.* **43**:1562.
8. PECORA, R. 1968. *J. Chem. Phys.* **48**:4126.
9. CUMMINS, H. Z., N. KNABLE, AND Y. YEH. 1964. *Phys. Rev. Letters* **12**:150.
10. DUBIN, S. B., J. H. LUNACEK, and G. B. BENEDEK. 1967. *Proc. Natl. Acad. Sci. U.S.A.* **57**:1164.
11. ARECCHI, F. T., M. GIGLIO, and U. TARTARI. 1967. *Phys. Rev.* **163**:186.
12. OSTER, G., P. M. DOTY, and B. H. ZIMM. 1947. *J. Amer. Chem. Soc.* **69**:1193.
13. FORRESTER, A. T., R. A. GUDMUNDSEN, and P. O. JOHNSON. 1955. *Phys. Rev.* **99**:1691.
14. FORRESTER, A. T. 1961. *J. Opt. Soc. Amer.* **51**:253.
15. GLAUBER, R. J. 1963. *Phys. Rev.* **130**:2529. **131**:2766.
16. GLAUBER, R. J., C. DE WITT, A. BLANDIN AND C. COHEN-*Tannoudji* 1965. *In* Quantum Optics and Electronics. C. DeWitt, editors. Gordon & Breach Science Pubs., Inc., New York.
17. GLAUBER, R. J. 1966. *In* Physics of Quantum Electronics Conference proceedings. P. L. Kelley, B. Lax, and P. E. Tannenwald, editors. McGraw-Hill Book Company, New York. 788.
18. MANDEL, L. 1963. *In* Progress in Optics. E. Wolf, editor. John Wiley & Sons, Inc., New York. **2**:183.
19. MANDEL, L., and E. WOLF. 1965. *Rev. Mod. Phys.* **37**:231.
20. FORD, JR., N. C., and G. B. BENEDEK. 1965. *Phys. Rev. Letters* **15**:649.
21. ALPERT, S. S., Y. YEH, and E. LIPWORTH. 1965. *Phys. Rev. Letters* **14**:486.
22. ALPERT, S. S. 1966. *In* Physics of Quantum Electronics. Conference proceedings. P. L. Kelley, B. Lax, and P. E. Tannenwald, editors. McGraw-Hill Book Company, New York. 253.
23. TANFORD, C. 1961. Physical Chemistry of Macromolecules. John Wiley & Sons, New York. pp. 327 and 436.
24. BOEDKER, H., and N. S. SIMMENS. 1958. *J. Amer. Chem. Soc.* **80**:2550.
25. CASPER, D. L. D. 1963. *Advan. Protein Chem.* **18**:37.

26. HALL, C. E. 1958. *J. Amer. Chem. Soc.* **80**:2556.
27. WILLIAMS, R. C., and R. L. STEERE. 1951. *J. Amer. Chem. Soc.* **73**:2057.
28. O'KONSKI, C. T., and A. J. HALTNER. 1956. *J. Amer. Chem. Soc.* **78**:3604.
29. STEERE, R. L. 1963. *Science.* **140**:1089.
30. ACKERS, G. K., and R. L. STEERE. 1967. *In* Methods in Virology. K. Maramorosch and H. Koprowski, editors. Academic Press, Inc., New York. **2**:325.
31. TRIEBEL, H., H. VENNER, and W. KAYSER. 1961. *Z. Naturforsch.* **16b**:308.